Introduction

Icing phenomena on an aircraft can occur when atmospheric conditions are below the freezing point of water, and supercooled water droplets are present in the air. Icing is characterized by ice accretion on the exposed surfaces like the wings' leading edges or nacelles' inlets. The consequences of such parasite accretions are harmful for the aircraft performance: increase in weight and drag, decrease in lift and handling or obstruction of vital sensors such as the Pitot tubes. This can lead to catastrophes and fatal accidents, as described by Petty and Floyd (2004). Even if icing incidents represented only 0.4% of the number of airplanes incidents over the period 1997–2006, they accounted for an impressive 13% of weather-related incidents over the same period (Jones, Reveley, Evans, & Barrientos, 2008).

To face this threat against safety, certification procedures include an icing component (Habashi, Tran, Baruzzi, & Benquet, 2003). Flight tests are mandatory to assess the capabilities of an aircraft to fly in icing conditions, but numerical simulations became a major tool to predict icing phenomena earlier in the design phase (Skeen Jr & Reed, 2004). These simulations allow predicting the characteristics of the ice accretion, the more interesting aspect being the geometrical shape of the ice block. These predictions can lead to a better understanding of the aerodynamic degradation caused by the ice (Bragg, Broeren, & Blumenthal, 2005). To numerically simulate an ice accretion on a geometry, four models are involved: the flow field model (by computational fluid dynamics (CFD)), the water droplets impacts locations model, the ice growth model, and the geometry update model (Beaugendre, Morency, & Habashi, 2006). The main topic of the present article lies in the third point: compute the ice growth and shape. Icing is a complex phenomenon where solid ice can coexist with a water film flow. Generally, during an accretion without de-icing heating, a moving liquid film, also called runback water, surmounts the ice layer lying on the airfoil. This flow plays a major role in the icing process. Such computation involves a coupling between aerodynamics (obtained by CFD) and heat transfer between the airfoil, the air and the water and/or ice on the airfoil's surface. The pioneer in the domain of numerical icing simulation was Messinger (1953), who proposed a mass and energy balance to be able to estimate the growth rate of the accretion. This original model is based on simplifying assumptions like neglecting heat transfer in the ice layer or being a steady model. Nevertheless, it is still used as a starting point for more recent models. Recent implementations done by Myers (2001) or Zhu et al. (2012) improve the capabilities of the Messinger model by adding features like conduction in the layers or unsteadiness. Meanwhile, especially since the 2000s, other models have also been implemented derived from the Messinger model, for example the Shallow Water Icing Model, called SWIM (Bourgault, Beaugendre, & Habashi, 2000). This model is based, among others, on the assumption that the velocity inside the water film is zero at the water/ice interface, and equals the flow shear stress at the air/water interface. Comparisons made by Lavoie et al. (2018) allows confronting these models. Their conclusions tend to show that for the same test case, ice accretion results may vary depending on the model chosen for the simulation. These differences are due to the multiple approaches and simplifications depicted

previously, such as conduction through ice taken into account in some models and not the others, for example.

To anticipate how to get rid of accreted ice, de-icing models have also been developed. Thermal de-icing systems generate heat with an electro-thermal device or blow hot air in the inside of the leading edge. This aspect related to icing is also part of the simulation process. Chauvin et al. (2014) propose a methodology to model this de-icing process. This involves generally a heat source inside the wing to simulate a de-icing heater and study heat transfer leading to ice melting, and finally ice block shedding. Studying this melting process can lead to more efficient de-icing devices' designs (Pourbagian & Habashi, 2015), in a period when energy efficiency became a preponderant aspect in aerospace industry. The present paper focuses on the implementation of an ice accretion model and the sensitivity study of the roughness model on the ice shape. The objective of the paper is to quantify the ice shape's geometry differences obtained using different rough thermal boundary layer's corrections. Analysis will study the differences in heat transfer coefficient resulting from various rough thermal corrections, and how these variations quantitatively affect the ice shape. Results will highlight the ice profiles obtained on a 2D test case on a NACA0012 airfoil. First part of the paper will describe the numerical models implemented for icing simulations. Afterwards, a 2D verification test case around a NACA0012 airfoil will be shown prior to show the results and analysis. The results will consist of plotting ice shapes' profiles accreted for different roughness models. Then, the analysis will perform quantitative comparisons between the geometrical characteristics of the ice blocks.

Model and methodology

Icing simulation

Most icing codes are relying on the Messinger model and its more recent improvements. In the present study, a model inspired by the original Messinger model (1953) and well detailed by Özgen and Canibek (2008) is implemented. This model is based on a mass and an energy balances computed in a control volume at the surface of the airfoil. The following figure shows a scheme of the domain used for such a simulation.

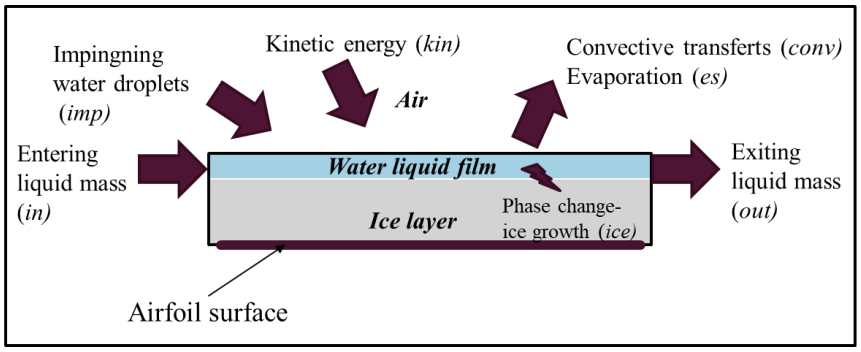

Figure 1: Scheme of the icing problem in the Messinger formulation

In the retained formulation, a set of two main equations, the mass balance and the energy balance govern the problem, respectively:

$$\dot{m}_{in} + \dot{m}_{imp} - \dot{m}_{ice} - \dot{m}_{es} - \dot{m}_{out} = 0 \quad (1)$$

$$\dot{Q}_{conv} + \dot{Q}_{es} + \dot{Q}_{imp} - \dot{Q}_{kin} - \dot{Q}_{ice} - \dot{Q}_{in} = 0 \quad (2)$$

The subscripts in equations (1) and (2) are depicted in the previous Figure 1. Another parameter used in the model is the freezing fraction, which quantifies the proportion of incoming water that freezes on the surface. This quantity is then between 0 (all of the water stays liquid) and 1 (all of the water freezes). The expression for the freezing fraction is the following:

$$f_{ice} = \frac{\dot{m}_{ice}}{\dot{m}_{in} + \dot{m}_{imp}} = \frac{\dot{m}_{ice}}{\dot{m}_{in} + LWC \cdot \beta \cdot V} \quad (3)$$

The definition of the freezing fraction allows reformulating equation (1) as:

$$\dot{m}_{out} = (1 - f_{ice})(\dot{m}_{in} + LWC \cdot \beta \cdot V) \quad (1b)$$

All the energy terms involved in the previous equations are well described by Özgen and Canibek (2008) :

$$\dot{Q}_{conv} = h_c(T_s - T_{rec}) \quad (4)$$

$$\dot{Q}_{es} = \frac{0.622 h_c e_o \, (T_s - T_a)}{C_{p,air} P_t L_e^{\frac{2}{3}}} (L_S + L_E) \qquad (5)$$

$$\dot{Q}_{imp} = LWC \cdot \beta \cdot V \cdot C_{pw}(T_s - T_a) \qquad (6)$$

$$\dot{Q}_{kin} = LWC \cdot \beta \cdot \frac{V^3}{2} \qquad (7)$$

$$\dot{Q}_{ice} = \dot{m}_{ice} \cdot L_F \qquad (8)$$

$$\dot{Q}_{in} = \dot{m}_{in} \cdot C_{pw}(T_s - T_a) \qquad (9)$$

All the constants involved in the equations are detailed in the nomenclature at the beginning of the paper. The recovery temperature involved in the convective term computation is obtained with equation (10):

$$T_{rec} = T_a(1 + Pr^{1/3} \cdot 0.2M^2) \qquad (10)$$

The collection efficiency β cited previously is a quantity characterizing the capacity of the airfoil geometry to "catch" the water droplets present in the air. The following figure 2 gives the collection efficiency of a NACA0012 airfoil, at 0 and 4-degree angle of attack, with respect to the non-dimensional curvilinear position on the airfoil. The data used are from Özgen and Canibek (2008).

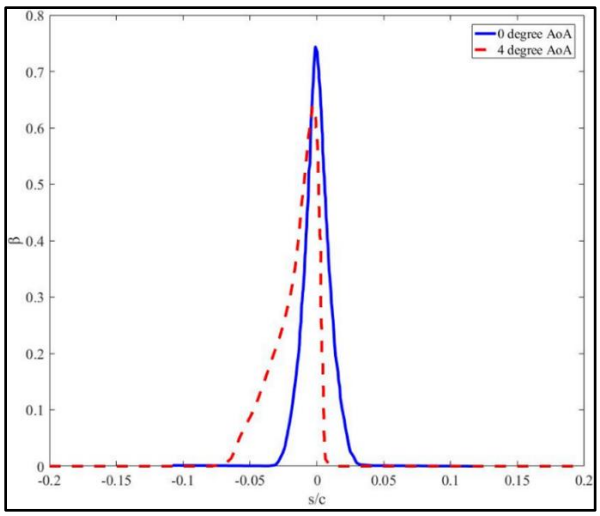

Figure 2: Collection efficiency for a NACA0012 airfoil (Adapted from Özgen and Canibek, 2008)

The computation of the ice thickness uses the algorithm illustrated on the following Figure 3. To solve the Messinger equations, a loop is performed on the cells at the airfoil surface. The size of the cells in the chord wise direction is 0.25 mm.

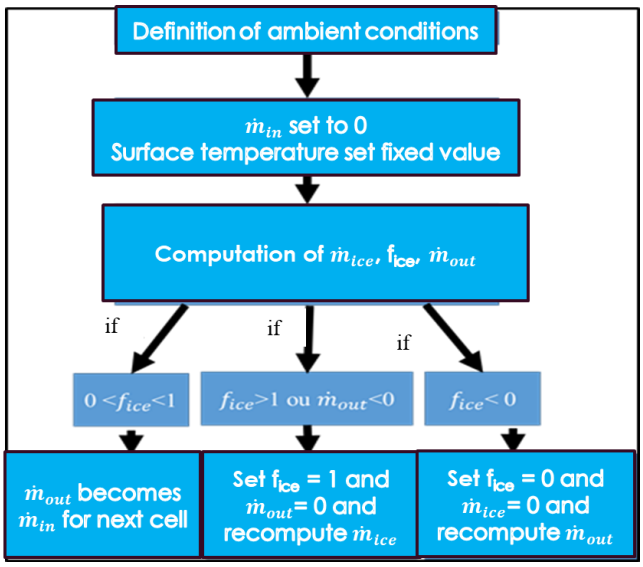

Figure 3: Algorithm of the ice accretion code

Sensitivity of h_c to the roughness model

The main topic of the present paper is the sensitivity of the ice shape to the heat transfer coefficient h_c. This coefficient plays a major role in the ice accretion process since the convective term in the energy equation (2) is, with the ice growth term, the most preponderant (E. Newton, James Vanfossen, Poinsatte, & J. Dewitt, 1988). In the present

study, three thermal boundary layer corrections due to roughness will be compared. It will be shown later that these models have an influence on h_c, and hence on the ice shape. The equivalent sand grain roughness for the simulations is k = 590 µm. The selected flow parameters make a fully rough regime.

The first rough simulation is used without any correction, this configuration will be called *None*. The second model uses the boundary layer correction from Aupoix (2015) and will be referred as the *HAX*. Finally, the last case studied uses the correction case from Kays and Crawford (1993), this case will be denoted as *HKC*. For flows on a rough surface, it has been shown that the logarithmic velocity profile in the boundary layer is shifted downwards compared to a smooth case (Olazabal-Loumé, Danvin, Julien, & Aupoix, 2017). The gap between the smooth logarithmic profile and the rough one is denoted Δu^+, see Figure 4.

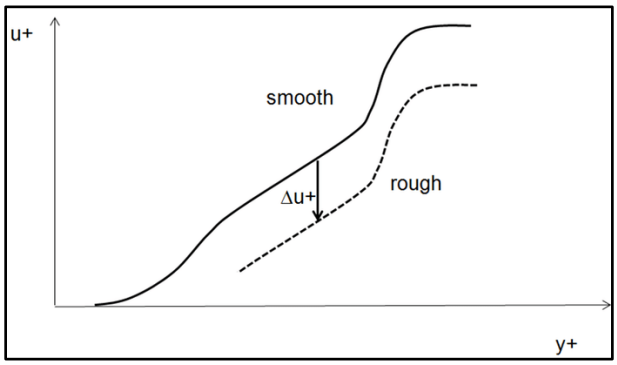

Figure 4: Shifting of velocity profile in a rough case, adapted from Olazabal-Loumé et al., 2017

The corrections suggested by Aupoix (2015) and Kays and Crawford (*HKC*) give estimations of Δu^+. These corrections are given in equations (11) and (12) for *HAX* and *HKC* cases, respectively. Similar shifts are observed for the temperature profile: the correction from Aupoix (2015) is given by equation (13), using a Prandtl number correction, and the one from Kays and Crawford (1993), using a ΔT^+ correction characterizing the temperature shift, in equation (14).

$$\Delta u^+(k_s^+) = \frac{1}{\kappa}\ln(k_s^+) - 2.98 \tag{11}$$

$$\Delta u^+(k_s^+) = \frac{1}{\kappa}\ln\left(1 + \frac{k_s^+}{e^{1.3325}}\right) \tag{12}$$

$$Pr_{total} = Pr + \left(A \cdot \Delta u^{+} + B \cdot \Delta u^{+2}\right) \exp\left(-\frac{y}{k}\right) \quad (13)$$

$$\Delta T^{+} = \frac{1}{\kappa_\theta} \ln\left(\frac{k_s^{+}}{32.6}\right) + C_\theta(Pr) - 1.25 Pr^{0.44} k_s^{+0.2} \quad (14)$$

A and B are coefficients given by Aupoix (2015). In both cases, k_s^+ denotes the non-dimensional roughness height, calculated as:

$$k_s^{+} = \frac{k \cdot u_\tau}{\mu} \quad (15)$$

With u_τ the friction velocity and μ the dynamic viscosity of air.

The use of the different roughness models gives different values of h_c around a NACA0012 airfoil. The value of the heat transfer coefficient versus the non-dimensional curvilinear abscissa *s/c* for each rough model and the smooth airfoil is plotted on the Figure 5.

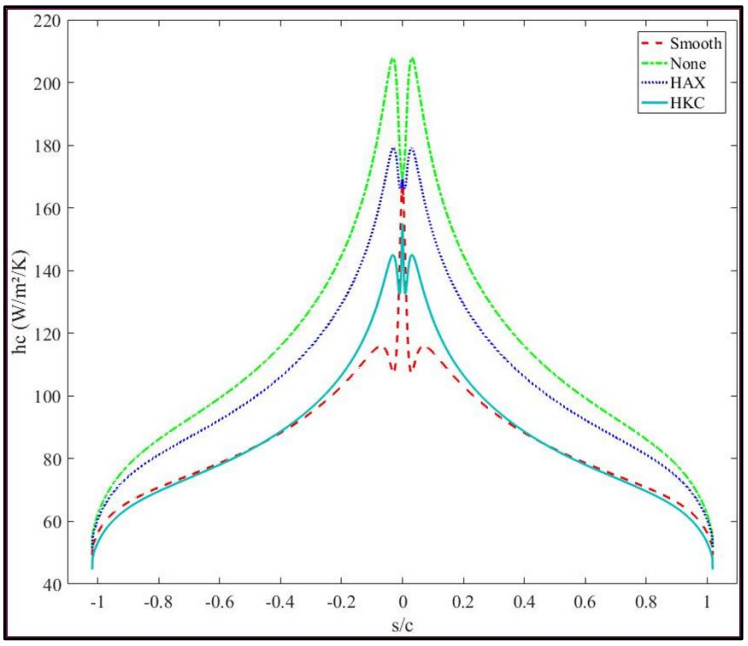

Figure 5: h_c around a NACA0012 airfoil

It is possible to quantify the differences in h_c resulting from the roughness model: the correction given for the *None* case overestimate the value of the coefficient compared to the *HAX* and *HKC* models cases. Nevertheless, the rough airfoil, whatever the correction,

has a higher heat transfer coefficient than the smooth one. The differences are summed up in the next Table 1, where the smooth case is taken as a reference for relative differences calculations.

Table 1: Comparisons between the characteristics of h_c for different roughness models

Model	**Smooth**	***None***	***HAX***	***HKC***
Mean value (airfoil)	99,6 W/m²/K	133,5 W/m²/K	122,2 W/m²/K	102,1 W/m²/K
Mean value (first 15% of the airfoil)	131,3 W/m²/K	182,8 W/m²/K	165,8 W/m²/K	137,5 W/m²/K
Max value	167,6 W/m²/K	207,9 W/m²/K	179,2 W/m²/K	155 W/m²/K
Mean difference vs. Smooth	-	34%	22,7%	2,5%

The next section will present the results of ice accretion obtained using these roughness models on a NACA0012 test case.

Results

Verification

To verify the code, results from the literature will be compared. Results from Lavoie et al. (2018) around a NACA0012 airfoil will be the reference for literature comparison. The parameters of the test case are summarized in the following table.

Table 2: Values for the icing test case

Parameter	**Value**
Chord length	0.53 m
Angle of attack	4°
Free stream velocity	58.1 m/s
Ambient air temperature	269.1 K
Wall temperature	273.15 K
Ambient pressure	95610 Pa
Liquid water content	1.3 g/m^3
Icing time	480 s
Air density	1.238 kg/m^3

Prior to compare to the literature, a straightforward test case is run to ensure that the code presents the same ice block profile in a rime ice situation. Rime ice situation occurs when

the temperature is low enough so that all of the incoming water freezes on the airfoil. To study this case, simulations with the different roughness models depicted in the previous section have been compared. For this rime ice case, the ambient temperature has been set to 230 K. The ice profile is presented on the Figure 6.

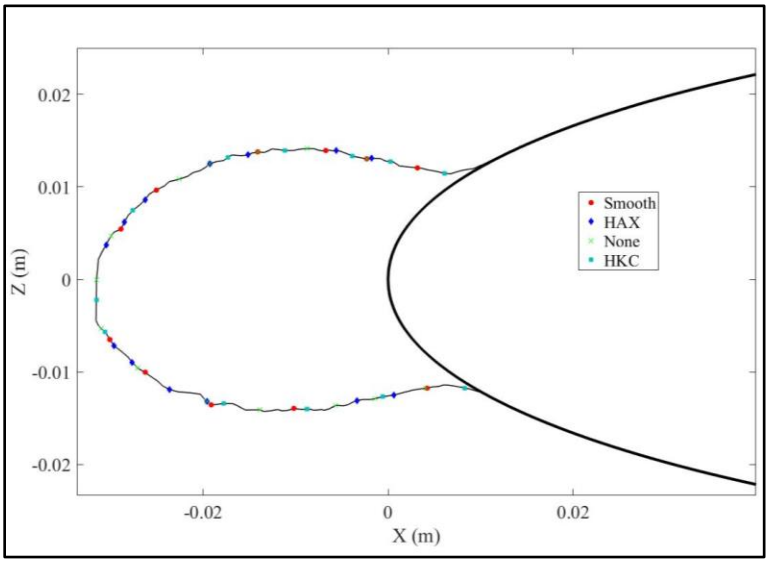

Figure 6: Rime ice comparison

It is possible to see that the code works as expected: all of the ice profiles are the same and do not depend on the convective effects, since all of the incoming water freezes. The freezing fraction is uniformly 1 on the surface.

The results obtained for the glaze ice test case are presented in the following Figure 7. The "step" shape of the end limit of the ice block is due to the single layer approach and the quite sharp decrease to zero of the collection efficiency presented previously on Figure 2. The size of the cells used to solve the Messinger equations is 0.25 mm in the chord wise direction. The runback water flow is occurring during the whole process (f_{ice} <1) since the conditions corresponds to glaze ice formation.

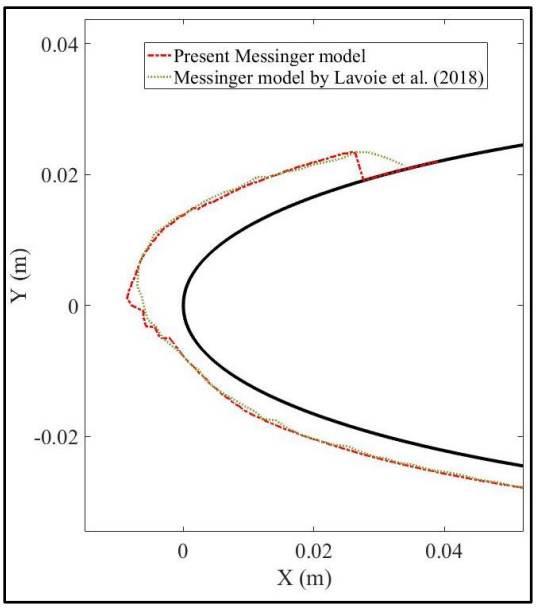

Figure 7: Comparison between the ice accretion of the present model and the literature

Results compare well with the literature, despite little differences at the stagnation point and the end of the ice block. These differences may be due to unknown parameters in the reference from Lavoie et al. (2018), for example the collection efficiency β that is not given. For the present simulation, the collection efficiency at 4° angle of attack previously shown in Figure 2 has been used.

Glaze Ice *Roughness Model Sensitivity Analysis*

Now the model is verified and present satisfactory results, simulations can be done using different models of heat transfer roughness correction in a glaze ice situation. This situation differs from the rime ice case by having higher temperature, closer to 273 K, which allows liquid and solid water to coexist. The parameters for the test case are summed up in the Table 3 below.

Table 3: Glaze ice test case parameters

Parameter	**Value**
Chord length	0.53 m
Angle of attack	0°
Free stream velocity	62.92 m/s
Ambient air temperature	264.5 K
Wall temperature	273.15 K
Ambient pressure	49191 Pa
Liquid water content	1.3 g/m^3
Icing time	480 s
Air density	0.648 kg/m^3

The results obtained with the different roughness models are shown in Figure 8.

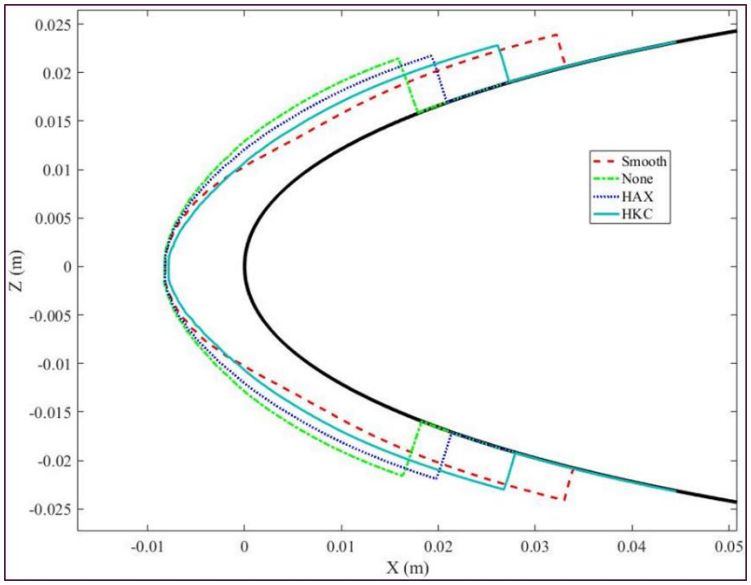

Figure 8: Ice profiles comparison between the different roughness models

As expected, the ice block shape is sensitive to the value of h_c that differs from one model to another. Although the maximum thickness at the stagnation point is close, the main differences are in the mean thickness and the ice extension on the leading edge. The following table quantifies these differences, where the smooth case is taken as a reference for the relative differences. The "ice extension on leading edge" is taken to make an analogy with the "main accretion area" measured by NASA during their study (Anderson & Tsao, 2008).

Table 4: Glaze ice characteristics comparison

Model	**Thickness at stagnation point**	**Thickness difference at stagnation point**	**Ice extension on leading edge**	**Extension difference**	**Mean thickness**	**Mean thickness difference**
Smooth	8,17 mm	-	93,8 mm	-	3,35 mm	-
None	8,26 mm	1,1%	59,8 mm	36%	5,18 mm	54,6%
HAX	8,2 mm	0,4%	66,7 mm	29%	4,66 mm	39,1%
HKC	7,83 mm	4,1%	81 mm	14%	3,82 mm	14%

The figures in Table 4 show that the differences observed in Table 2 for the h_c are reflected on the main characteristics of the ice formation. Globally, the differences are amplified: a 34% difference in the heat transfer coefficient from smooth to *None* cases results in a decrease of 36% of the ice extension and a 54.6% of increase in the mean thickness. Nevertheless, the global ice mass is conserved because the incoming water quantities remain the same. This amplification is also observed for the *HAX* and *HKC* cases when compared to the smooth configuration. Future investigations will be carried to evaluate the models in other test cases by varying the freestream temperature and other flow field characteristics to perform more complex sensitivity tests.

Conclusions

In the present study, a Messinger icing model has been implemented to study the effect of heat transfer roughness model on the final ice shape on a NACA0012 airfoil. The results show different values of the heat transfer coefficient depending on the roughness model chosen. These differences impact on the glaze ice shape's characteristics such as the mean thickness and the extension of the ice block on the leading edge. It is observed that the relative differences in the h_c values are amplified in the geometrical differences of ice shape. For instance, a difference of only 2.5% of the mean value of h_c around a NACA0012 implies a difference of 14% in mean ice thickness and extension. Future improvements of the icing code will be the deeper investigation of roughness models for boundary layer corrections, in order to propose a model that provides more accurate results compared to experimental data.

Acknowledgements

The authors would like to thank the *Décanat Des Études de l'École de technologie supérieure* and the association *Le Tomato- Aéroclub de France* for the funding of the project.

References

Anderson, D. N., & Tsao, J.-C. (2008). *Ice Shape Scaling for Aircraft in SLD Conditions*.

Aupoix, B. (2015). Improved heat transfer predictions on rough surfaces. *International Journal of Heat and Fluid Flow, 56*, 160-171. doi: https://doi.org/10.1016/j.ijheatfluidflow.2015.07.007

Beaugendre, H., Morency, F., & Habashi, W. G. (2006). Development of a second generation in-flight icing simulation code. *Journal of Fluids Engineering, 128*(2), 378-387. Repéré à https://hal.inria.fr/inria-00337571

Bourgault, Beaugendre, & Habashi. (2000). Development of a Shallow-Water Icing Model in FENSAP-ICE. *Journal of Aircraft, 37*(4), 640-646. doi: 10.2514/2.2646

Bragg, M. B., Broeren, A. P., & Blumenthal, L. A. (2005). Iced-airfoil aerodynamics. *Progress in Aerospace Sciences, 41*(5), 323-362. doi: https://doi.org/10.1016/j.paerosci.2005.07.001. Repéré à http://www.sciencedirect.com/science/article/pii/S0376042105000801

Chauvin, R., Villedieu, P., & Trontin, P. (2014). A robust coupling algorithm applied to thermal ice protection system unsteady modeling. Dans *6th AIAA Atmospheric and Space Environments Conference - AVIATION 2014*. Repéré à https://hal.archives-ouvertes.fr/hal-01088749

E. Newton, J., James Vanfossen, G., Poinsatte, P., & J. Dewitt, K. (1988, 1988). *Measurement of local convective heat transfer coefficients from a smooth and roughened NACA-0012 airfoil: Flight test data* présentée à 26th Aerospace Sciences Meeting, Reno, Nevada.

Habashi, W., Tran, P., Baruzzi, G., & Benquet, M. (2003). *Design of Ice Protection Systems and Icing Certification Through the FENSAP-ICE System*.

Jones, S. M., Reveley, M. S., Evans, J. K., & Barrientos, F. A. (2008). *Subsonic Aircraft Safety Icing Study* (nº NASA/TM--2008-215107, L-19435). Hampton, VA, United States: NASA.

Kays, W. M., & Crawford, M. E. (1993). *Convective heat and mass transfer*.

Lavoie, P., Pena, D., Hoarau, Y., & Laurendeau, E. (2018). Comparison of thermodynamic models for ice accretion on airfoils. *International Journal of Numerical Methods for Heat & Fluid Flow, 28*(5), 1004-1030. doi: doi:10.1108/HFF-08-2016-0297

Messinger, B. L. (1953). Equilibrium Temperature of an Unheated Icing Surface as a Function of Air Speed. *Journal of the Aeronautical Sciences, 20*(1), 29-42. doi: 10.2514/8.2520

Myers, T. G. (2001). Extension to the Messinger Model for Aircraft Icing. *AIAA Journal, 39*(2), 211-218. doi: 10.2514/2.1312

Olazabal-Loumé, M., Danvin, F., Julien, M., & Aupoix, B. (2017). *Study on k-w shear stress transport model corrections applied to rough wall turbulent hypersonic boundary layers*. doi: 10.13009/EUCASS2017-604

Özgen, S., & Canıbek, M. (2008). Ice accretion simulation on multi-element airfoils using extended Messinger model. *Heat and Mass Transfer, 45*(3), 305. doi: 10.1007/s00231-008-0430-4

Petty, K. R., & Floyd, C. D. J. (2004). *A statistical review of aviation airframe icing accidents in the U.S.*

Pourbagian, M., & Habashi, W. G. (2015). Aero-thermal optimization of in-flight electro-thermal ice protection systems in transient de-icing mode. *International Journal of Heat and Fluid Flow, 54*, 167-182. doi: https://doi.org/10.1016/j.ijheatfluidflow.2015.05.012. Repéré à http://www.sciencedirect.com/science/article/pii/S0142727X15000582

Skeen Jr, J. T., & Reed, S. L. (2004). *Weather-related aviation accident investigations at the national transportation safety board* présentée à 11th Conference on Aviation, Range, and Aerospace Meterology, October 4, 2004 - October 8, 2004, Hyannis, MA, United States.

Zhu, C., Fu, B., Sun, Z., & Zhu, C. (2012). 3D Ice Accretion Simulation For Complex Configuration Basing On Improved Messinger Model. *International Journal of Modern Physics: Conference Series, 19*, 341-350. doi: 10.1142/s2010194512008938